3.2. DNA-Template Construction for Transcription

Cap and poly A (pA), found on almost all eukaryotic mRNAs, stimulate translation initiation and stabilize mRNA by their synergistic action. However, for in vitro translation the use of cap and pA can be a major problem *(4)*. This has been effectively overcome by inserting optimized 5'- and 3'-untranslated regions (UTRs) upstream and downstream from the coding regions *(4)*. Optimized 5'- and 3'-UTRs can be fused to the gene of interest in two different ways: (1) by cloning the same gene in a plasmid vector carrying the proper UTRs and then amplifying the gene attached to 5'- and 3'-UTRs from the plasmid, and (2) by fusing the 5'- and 3'-UTRs during the amplification reaction from cDNAs. The optimized elements are assembled into a pSP65-derived vector called pEU (**Fig. 1A,B**). By using this assembled vector, the desired genes can be expressed efficiently without cap and poly(dA/dT) *(4)*. Cloning of the desired gene into the pEU3b expression system is achieved by using standard methods. After confirming the DNA sequence, the plasmid containing the desired ORF is prepared by either the CsCl method *(5)* or by using small-scale plasmid preparation kits. Prior to mRNA synthesis, recombinant plasmid should be treated with phenol-chloroform to eliminate any RNases activity.

3.2.1. Template Preparation From pEU Carrying Optimized 5'- and 3'- UTRs

We have optimized a PCR-based linear template DNA preparation by designing a set of universal primers for pEU vector. The designed primers are SPu (5'- GCGTAGCATTTAGGTGACACT) and AODA2303 (5'- GTCAGACCCCGTAGAAAAGA). By using these primers, the desired DNA template can be easily generated and used directly for the preparation of mRNA without further purification as follows.

1. Prepare 100 µL of PCR reaction mixture as per the manufacturer's instructions (Takara) by mixing 100 pg/µL of plasmid and 200 n*M* of each primer, 200 µ*M* of each dNTP, and 1.25 U of ExTaq DNA polymerase.
2. Set the PCR thermo-cycler (Takara) on 1 min denaturation at 96°C followed by 25 cycles of amplification: 98°C for 10 s, 55°C for 30 s, and 72°C for 5 min depending on the length of the ORF (1 kb per min).

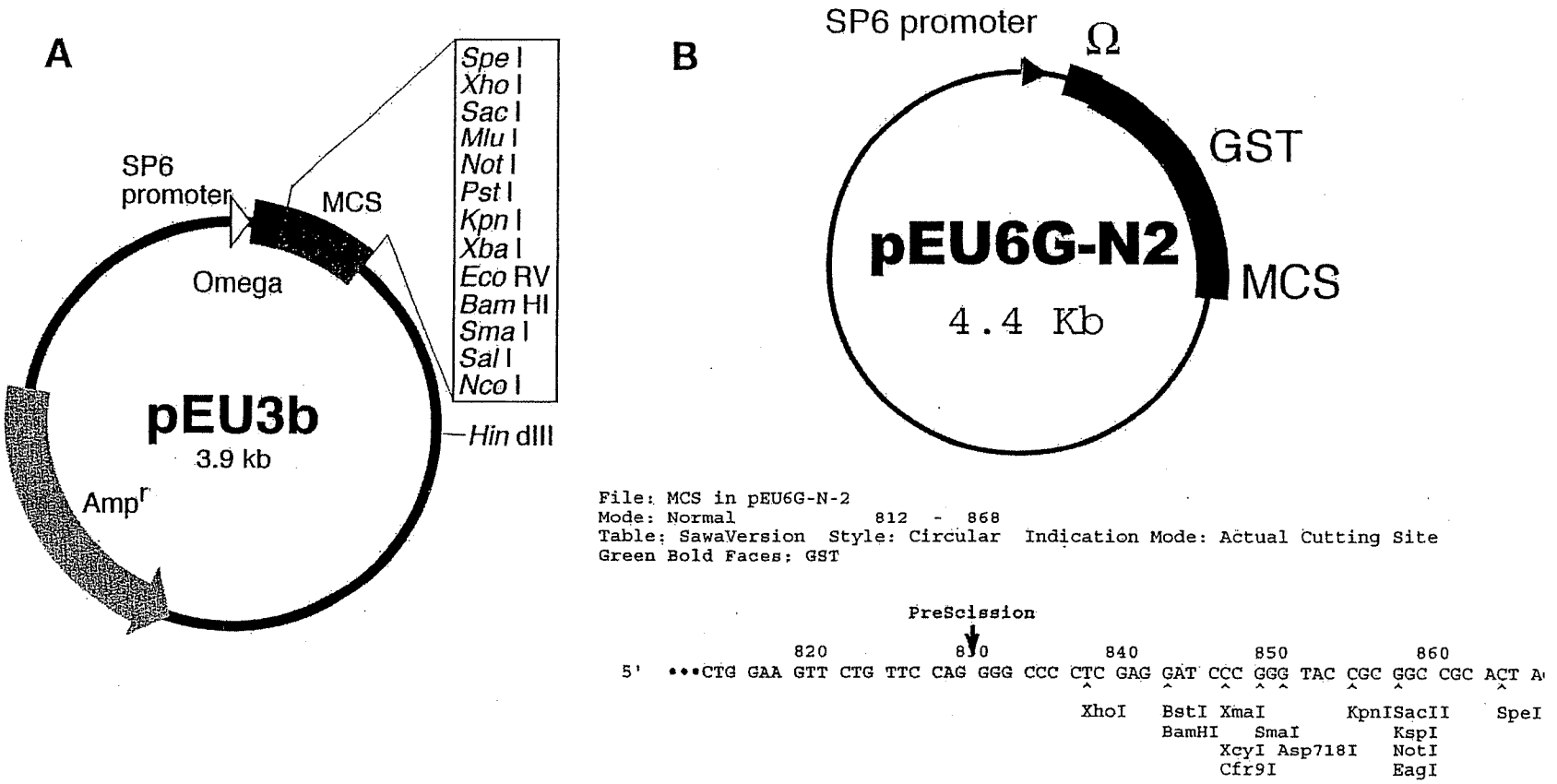

Fig. 1. (**A**) Schematic diagram of the pEU expression vector. (**B**) Map and sequence in multicloning site of pEU6G-N2 for GST-tag purification.

3. Concentrate the PCR product to approx 20 µL (~5 times) using Microcon according to the manufacturer's instructions.
4. After analyzing the integrity of DNA template by agarose gel electrophoresis, the template DNA is used for the transcription.

3.2.2. Direct Fusion of 5'- and 3-UTRs by Split-Primers PCR Technique

Because cloning of cDNA into an expression vector is one of the most laborious and time-consuming steps of the entire process, direct synthesis of the template by PCR is preferred *(6,7)*. This is achieved by the incorporation of transcriptional and translational start and stop signals into primers used for the amplification of the gene of interest. In this section, we focus on the construction of template DNA starting from cDNA clones by using the split-primers PCR technique *(4)*. The strategy is illustrated in **Fig. 2**.

3.2.2.1. Design of Primers

As shown in **Fig. 2**, split-primers PCR technique makes use of four primers:

1. The target specific primer (primer 3) is designed in such a way that its 3'-end can anneal to the 5'-end of the target gene and its 5'-end has part of the omega sequence *(4)*.
2. Primer 2 has the full-length omega sequence, thus allowing the annealing to the primer 3-derived amplification product and a part of the SP6 promoter sequence.
3. Primer 1 has the remaining part of the SP6 promoter and can anneal to primer 2-derived amplification product.
4. Primer 4 is specific for the gene-carrying vector and can anneal several hundreds of basepairs downstream from the 3'-end of the gene of interest.

Therefore, for each clone of cDNA, primer 3 is the only specific primer and the remaining primers are common for all cDNAs. The sequences of the promers used are reported below:

Primer 1: 5'-GCGTAGCATTTAGGTGACACT (the underlined sequence is the 5' half of the promoter).

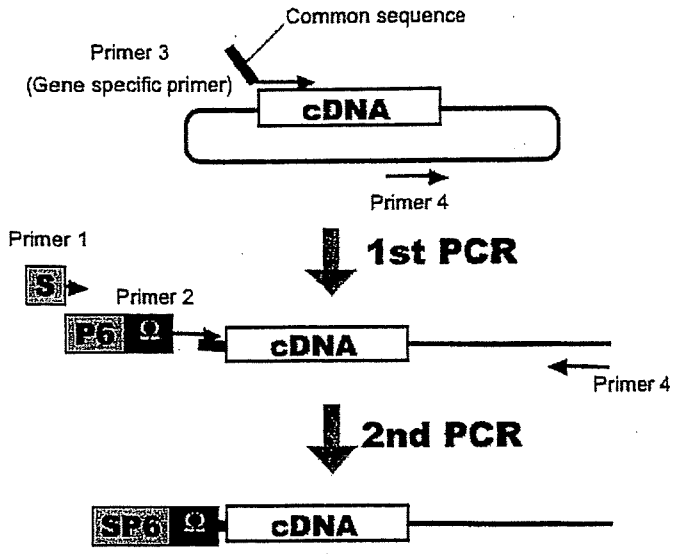

Fig. 2. Direct transcriptional template generation from cDNA library by using the split-primers PCR technique. A schematic representation of the split-primers design for equipping the cDNA sequences with the required UTRs.

Primer 2: 5'-*GGTGACACT*ATAGAAGTATTTTTACAACAATTAC CAACAACAACAACAAACAACAACAACATTACATTTTACATTCT ACAACTA*CCACCCACCACCACCAATG* (underlined is the 3'-half sequence of the promoter and the sequences in italic denote the region annealing to primer 1 and primer 3).

Primer 3: 5'-CCACCCACCACCACCAatgnnnnnnnnnnnnnnnn (the stretch of "ns" indicates the nucleotide sequence which is specific for the gene of interest).

Primer 4: 5'-AGCGTCAGACCCCGTAGAAA (based on the sequence of the vector plasmid described in **refs. *9–11***).

3.2.2.2. First PCR

1. Prepare 60 μL of a PCR reaction by mixing 3 ng of plasmid or 3 μL of an overnight culture of *Escherichia coli* carrying the plasmid, of dNTPs (200 μ*M* each), 1.5 U of ExTaq DNA polymerase, 10 n*M* of primer 3 and primer 4, and the polymerase buffer supplied by the manufacturer.

2. Set the PCR thermo-cycler on 4-min denaturation at 94°C followed by 30 cycles of amplification: 98°C for 10 s, 55°C for 30 s, and 72°C for 4–5 min, depending on the length of the gene (1 kb per min).

3.2.2.3. Second PCR

To attach the omega and SP6 promoter sequences to the first PCR product, a second 30 μL PCR was carried out by mixing 3 μL of the first PCR product (without any purification), 100 n*M* of primer 1 and 4, and 1 n*M* of primer 2 using the same amplification conditions as for the first PCR.

3.3. Sequential Transcription-Translation Reactions

Cell-free translation of proteins can be achieved mainly by three different modes, batch mode translation *(3,7)*, bilayer system *(8)*, and continuous-flow cell-free protein synthesis method *(4,9)*. Their basic concepts are described in our previous paper *(10)*. In this section, the bilayer mode of protein synthesis using unpurified mRNA will be explained in detail. **Table 1** summarizes the composition of the mixture, which varies depending on the amount of protein needed.

1. Prepare transcription reaction as indicated in **Table 1** except for wheat embryo extract and creatine kinase.
2. Incubate the reaction mixture at 37°C for 6 h.
3. Add 25 μL (250 μL for large scale [LS]) of wheat embryo extract, and 1 μL of 2 mg/mL creatine kinase (20 mg/mL creatine kinase for LS), and mix well (reaction mixture).
4. Prepare 550 μL (5.5 mL for LS) of TSB in the U-shaped titer plate well (six-well plate for LS).
5. Carefully transfer 50 μL (500 μL for LS) of the reaction mixture to the titer plate well by inserting the pipet tip down to the bottom of the well. Because of the higher density of the **step 3** mix compared with the **step 4** mix, one can clearly see two layers.
6. Place a sealing film and then a cover on the plate to avoid evaporation.
7. Keep the plate in an incubator at 26°C for 18 h without shaking.

Table 1
Reaction Mixture for Transcription and Translation

Reagen	Small scale (SS)	Large scale (LS)	Final concentration
Template DNA	*x* µL	*x* µL	1/5 vol (HC PCR)[a] 100 ng/µL (CP)[b]
5X TB	5	50	1X
25 m*M* NTP mix	2.5	25	2.5 m*M*
80 U/µL SP6 RNApolymerase	0.3	3	1 U/µL
80 U/µL RNasin	0.3	3	1 U/µL
Milli-Q	up to 24	up to 249	
Wheat embryo extract	25	250	120 A_{260}/mL
2 mg/mL creatine kinase	1	–	40 µg/mL
20 mg/mL creatine kinase	–	1	40 µg/mL

[a]Highly concentrated PCR product (>50 ng/mL).
[b]High quality circular plasmid.

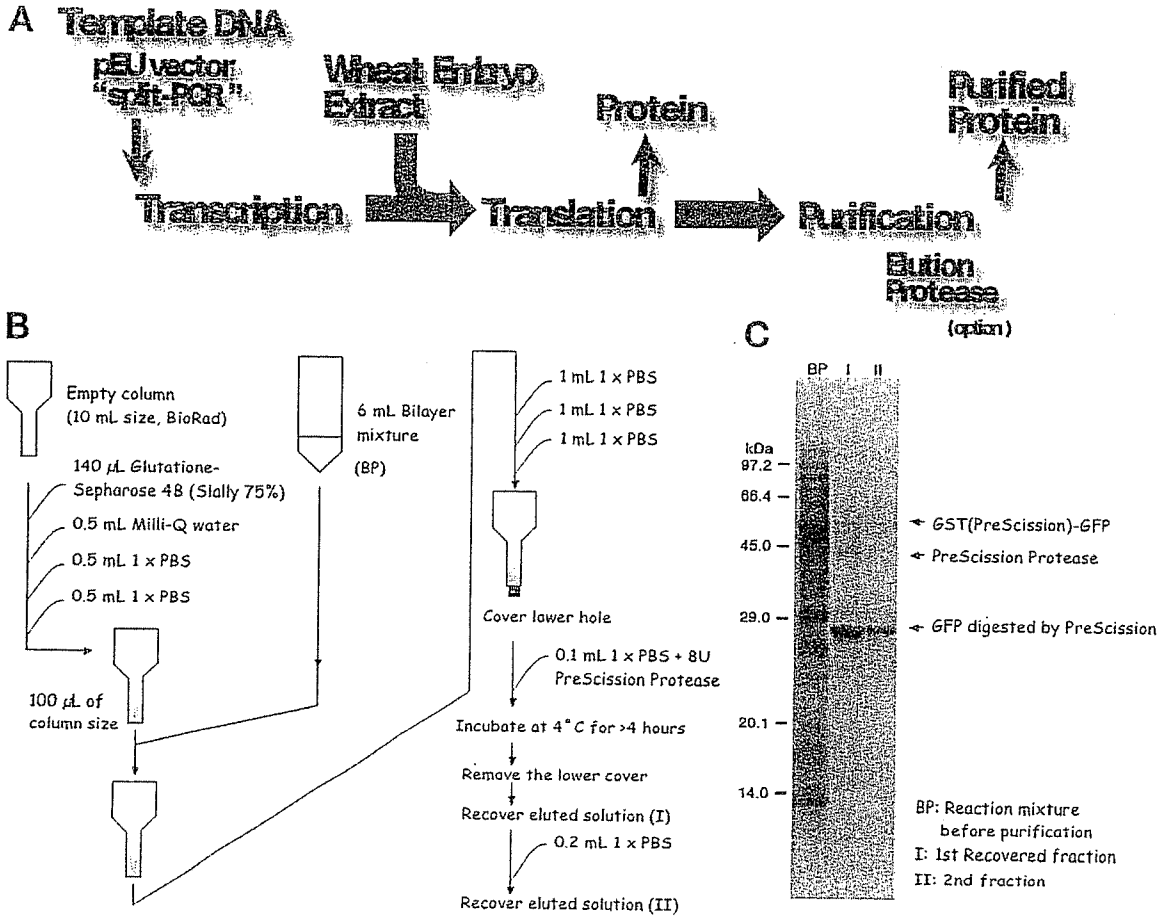

Fig. 3. (A) Flowchart of the cell-free production and purification process based on sequential transcription-translation reaction and purification. (B) Flowchart of protein purification by using GST-tag and on-column digestion with PreScission. (C) An example of purified protein.

3.4. Purification of Synthesized Protein by On-Column Digestion

This section describes the methods for (1) isolation of a GST-fused protein as obtained when a pEU-derived transcript is used (**Subheading 3.**), (2) removal of the GST moiety by PreScission protease, and (3) purification of the protein (*see* **Fig. 3B**,**C**).

1. Prepare the column (10 mL size) by adding 140 μL of glutathione-sepharose 4B resin.
2. Wash the column with 0.5 mL of Milli-Q water followed by 1 mL of 1X PBS.
3. Load 6 mL of the synthesized protein from **Subheading 3.3.** into the column.
4. Wash off the unbound proteins with 3 mL of 1X PBS.
5. Cap the bottom of the column.
6. Treat the column with 8 U PreScission protease in 0.1 mL of 1X PBS and then incubate at 4°C for 4 h.
7. Remove the cap and then elute the target protein without GST tag
8. Recover the target protein with 0.1 mL of 1X PBS one more time.

4. Notes

1. A possible procedure for the preparation of proteins can be:
   a. Selection and design of suitable genes from the data bank.
   b. Generation of template for the transcription by PCR, or by cloning into pEU.
   c. Transcription of mRNA.
   d. Translation in the wheat germ cell-free system.
   e. Fine tuning of translation conditions such as ion concentrations and incubation temperature for large-scale protein production.
   f. Purification of the product.

   Because the translation machinery prepared from wheat embryos are efficient and robust, we could in fact succeeded in the robotic automation of the processes from **steps c** through **f**.

References

1. Sawasaki, T., Hasegawa, Y., Morishita, R., Seki, M., Shinozaki, K., and Endo, Y. (2004) Genome-scale, biochemical annotation method based on the wheat germ cell-free protein synthesis system. *Phytochemistry* **65,** 1549–1555.
2. Vinarov, D. A., Lytle, B. L., Peterson, F. C., Tyler, E. M., Volkman, B. F., and Markley, J. L. (2004) Cell-free protein production and labeling protocol for NMR-based structural proteomics. *Nature Methods* **2,** 1–5.
3. Madin, K., Sawasaki, T., Ogasawara, T., and Endo, Y. (2000) A highly efficient and robust cell-free protein synthesis system prepared from wheat embryos: plants apparently contain a suicide system directed at ribosomes. *Proc. Natl. Acad. Sci. USA* **97,** 559–564.
4. Sawasaki, T., Ogasawara, T, Morishita, R., and Endo, Y. (2002) A cell-free protein synthesis system for high-throughput proteomics. *Proc. Natl. Acad. Sci. USA* **99,** 14,652–14,657.
5. Sambrook, J. and Russell, D. W. (2001) *Molecular Cloning: A Laboratory Manual, 3rd ed.* Cold Spring Harbor Laboratory Press, Cold Spring Harbor, NY.
6. Gurevich, V. V. (1996) Use of bacteriophage RNA polymerase in RNA synthesis. *Methods Enzymol.* **275,** 382–397.
7. Hanes, J. and Pluckthun, A. (1997) In vitro selection and evolution of functional proteins by using ribosome display. *Proc. Natl. Acad. Sci. USA* **94,** 4937–4942.
8. Sawasaki, T., Hasegawa, Y., Tsuchimochi, M., et al. (2002) A bilayer cell-free protein synthesis system for high-throughput screening of gene products. *FEBS Lett.* **514,** 102–105.
9. Spirin, A. S., Baranov, V. I., Ryabova, L. A., Ovodov, S. Y., and Alakhov, Y. B. (1988) A continuous cell-free translation system capable of producing polypeptides in high yield. *Science* **242,** 1162–1164.
10. Endo, Y. and Sawasaki, T. (2004) High-throughput, genome-scale protein production method based on the wheat germ cell-free expression system. *J. Struct. Funct. Genomics* **5,** 45–57.

JOURNAL OF VIROLOGY, Dec. 2008, p. 11958–11963
0022-538X/08/$08.00+0 doi:10.1128/JVI.01149-08

Vol. 82, No. 23

NOTES

Critical Role for TSLC1 Expression in the Growth and Organ Infiltration of Adult T-Cell Leukemia Cells In Vivo▽

M. Zahidunnabi Dewan,[1,2]† Naofumi Takamatsu,[3] Tomonori Hidaka,[4] Kinta Hatakeyama,[5] Shingo Nakahata,[3] Jun-ichi Fujisawa,[6] Harutaka Katano,[7] Naoki Yamamoto,[1,2]* and Kazuhiro Morishita[3]*

Department of Molecular Virology, Graduate School, Tokyo Medical and Dental University, 1-5-45 Yushima, Bunkyo-ku, Tokyo 113-8519, Japan[1]; AIDS Research Center, National Institute of Infectious Disease, 1-23-1 Toyama, Shinjuku-ku, Tokyo 162-8640, Japan[2]; Department of Medical Sciences,[3] Department of Internal Medicine,[4] and Department of Pathology,[5] Faculty of Medicine, University of Miyazaki, Kiyotake, Miyazaki, Japan; Department of Microbiology, Kansai Medical University, Moriguchi, Osaka, Japan[6]; and Department of Pathology, National Institute of Infectious Diseases, 1-23-1 Toyama, Shinjuku-ku, Tokyo 162-8640, Japan[7]

Received 2 June 2008/Accepted 15 September 2008

Adult T-cell leukemia (ATL) is associated with human T-cell leukemia virus type 1 infection. The tumor suppressor lung cancer 1 (TSLC1) gene was previously identified as a novel cell surface marker for ATL, and this study demonstrated the involvement of TSLC1 expression in tumor growth and organ infiltration of ATL cells. In experiments using NOD/SCID/γc^{null} mice, both leukemia cell lines and primary ATL cells with high TSLC1 expression caused more tumor formation and aggressive infiltration of various organs of mice. Our results suggest that TSLC1 expression in ATL cells plays an important role in the growth and organ infiltration of ATL cells.

Human T-cell leukemia virus type 1 (HTLV-1) is the causative agent of an aggressive form of $CD4^+$ T-cell leukemia termed adult T-cell leukemia (ATL) (7, 14, 18). Carriers of HTLV-1 have been identified in a number of locations throughout the world, including parts of Africa; Papua New Guinea; specific regions in Europe including Romania; parts of South America including northern Brazil, Peru, northern Argentina, and Colombia; and the southern part of Kyushu in Japan (17). Common findings in patients with ATL include enlargement of peripheral lymph nodes, hepatomegaly, splenomegaly, skin infiltration, and hypercalcemia. The Tax gene is a unique viral gene thought to play a central role in HTLV-1-induced transformation. It is responsible for transactivation of the HTLV-1 long terminal repeat (5, 16) and numerous cellular genes involved in T-cell activation and growth, including those encoding interleukin-2 (IL-2) (11) and the α chain of IL-2 receptor (IL-2Rα) (CD25, Tac) (1, 2). The long latency of ATL development suggests that multiple genetic events accumulate in HTLV-1-infected cells; however, the precise molecular mechanisms of ATL leukemogenesis following HTLV-1 infection have not been fully elucidated.

The tumor suppressor lung cancer 1 gene (TSLC1) at chromosome 11q23 has been identified as a tumor suppressor gene in non-small-cell lung cancer (9, 13). In contrast, it was recently found to be highly and ectopically expressed in acute-type ATL cells, most ATL cell lines, and HTLV-1-infected T-cell lines (15). Enforced expression of TSLC1 in ATL-derived ED-40515(−) cells resulted in higher aggregations and binding abilities in a human umbilical vein endothelial cell line (HUVEC). These results suggest that TSLC1 might contribute to tumor growth by enhancing aggregation after infiltration and migration outside blood vessels. Since the role of TSLC1 overexpression in the course of tumor growth and organ infiltration of ATL cells remains to be fully elucidated, we investigated the direct involvement of TSLC1 in the growth and infiltration of leukemia cells using C57BL/6J and NOD-SCID/γc^{null} (NOG) mice (4, 8).

In order to analyze the tumorigenicity of TSLC1 expression in leukemia cells, a murine IL-2-independent T-lymphoma cell line (EL4) injected into the intraperitoneum of syngeneic C57BL/6J mice was used as a model for ATL. EL4 cells were transfected with a pcDNA3 expression plasmid containing TSLC1, and transformant cells were selected by a limiting-dilution method in the presence of G-418. We also used EL4 cells expressing a green fluorescent protein-Tax fusion protein (EL4/GAX) (6) and parental EL4 (EL4/p) as a control. Expression of Tax protein in EL4 cells, a 38-kDa band of Tax protein in HUT102 cells, and a 64-kDa band of green fluorescent protein-Tax fusion protein in EL4/GAX cells were all

* Corresponding author. Mailing address for Naoki Yamamoto: AIDS Research Center, National Institute of Infectious Disease, 1-23-1 Toyama, Shinjuku-ku, Tokyo 162-8640, Japan. Phone: 81-3-5285-1111. Fax: 81-3-5285-1165. E-mail: nyama@nih.go.jp. Mailing address for Kazuhiro Morishita: Division of Tumor and Cellular Biochemistry, Department of Medical Sciences, Faculty of Medicine, University of Miyazaki, Kiyotake, Miyazaki, Japan. Phone: 81-9-8585-0985. Fax: 81-9-8585-2401. E-mail: kmorishi@med.miyazaki-u.ac.jp.

† Present address: Department of Pathology, New York University School of Medicine, 550 First Avenue, New York, NY 10016.

▽ Published ahead of print on 15 October 2008.

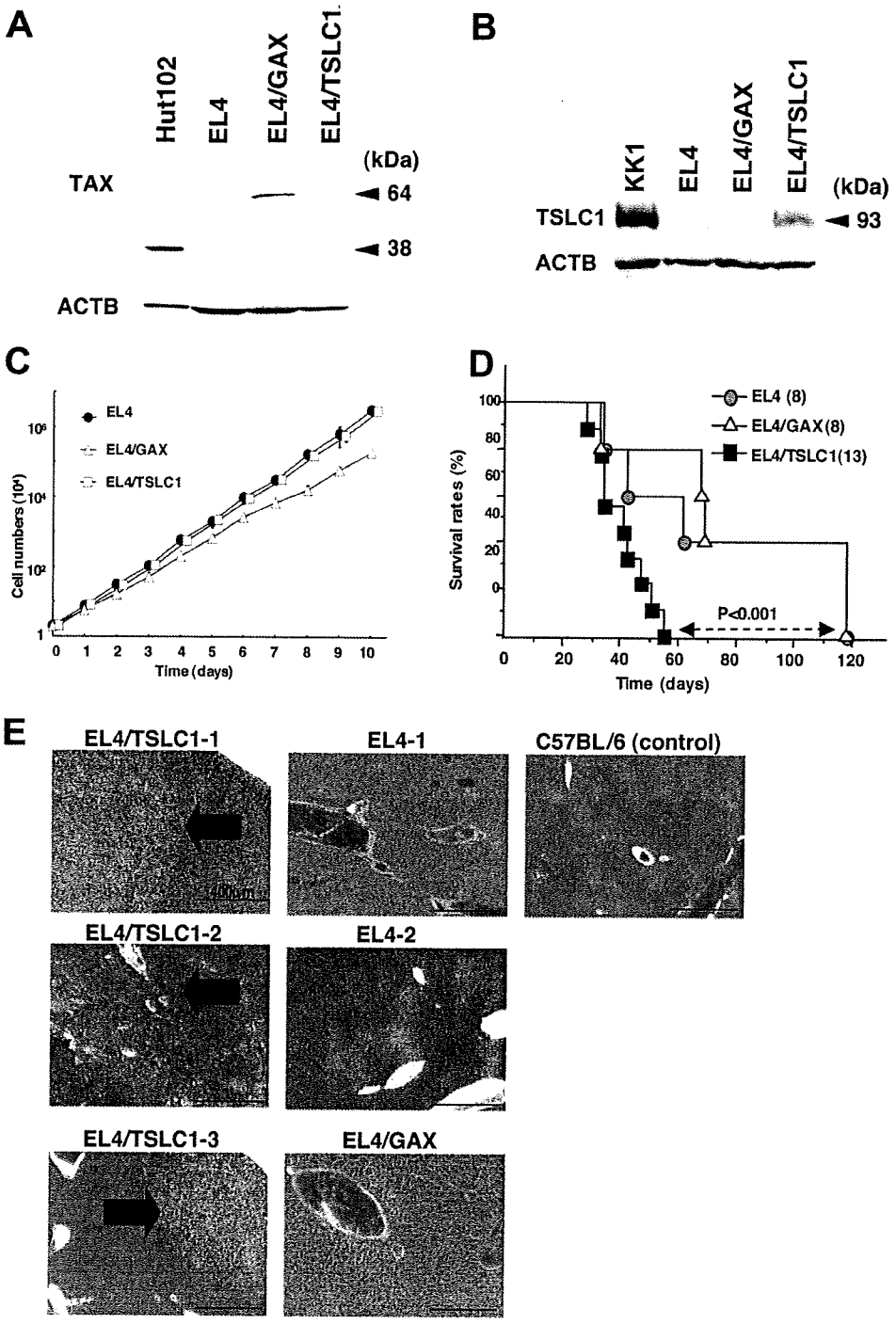

FIG. 1. Transplantation of EL4 T-cell lymphoma cells expressing TSLC1 shortened the life span of syngeneic mice. (A) Expression of Tax protein in HUT102, EL4, EL4/GAX, and EL4/TSLC1 cells was detected by Western blot analysis. Expression of β-actin protein (ACTB) was used as a loading control. (B) Expression of TSLC1 protein in KK1, EL4, EL4/GAX, and EL4/TSLC1 cells was detected by Western blot analysis. Expression of β-actin protein (ACTB) was used as a loading control. (C) Cell numbers in a growth curve are shown for an average of three independent counts, and standard deviations are indicated as error bars. (D) Survival curves of C57BL/6 mice inoculated in the abdominal cavity with EL4, EL4/GAX, or EL4/TSLC1 cells. Cumulative survival rates were calculated by the Kaplan-Meier method and compared using a log-rank test. (E) Liver sections from all mice were stained with hematoxylin-eosin. The regions of liver metastasis (arrow) were seen in liver sections from mice inoculated with EL4/TSLC1 cells but not shown in the liver sections from the mice inoculated with EL4 or EL4/GAX cells. Magnification, ×100; bars, 400 μm.

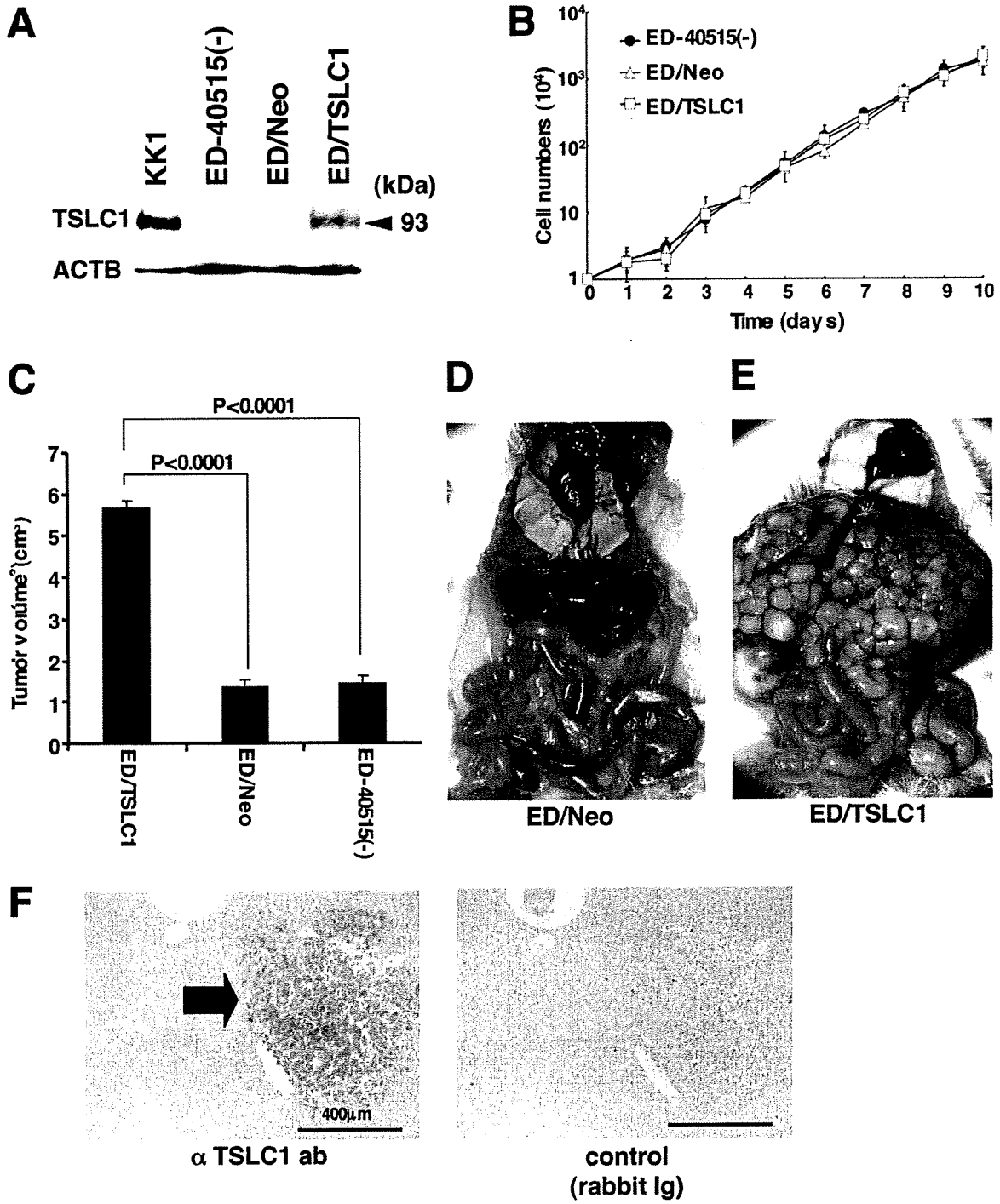

FIG. 2. Involvement of TSLC1 expression in tumor growth and infiltration of leukemia cells in NOG mice. (A) Expression of TSLC1 in KK1, ED-40515(−), ED/Neo, or ED/TSLC1 cell lines was detected by Western blot analysis. Expression of β-actin protein (ACTB) was used as a loading control. (B) Cell growth curves of ED-40515(−), ED/Neo, and ED/TSLC1 cell lines are shown for an average of three independent counts, and standard deviations are indicated as error bars. (C) Tumor volumes of mice inoculated subcutaneously with ED/TSLC1, ED/Neo, or ED-40515(−) cells after 21 days are shown as the means ± standard errors of the means for five mice in each group. Statistical analysis was done with a Student *t* test. (D and E) The pictures shown were derived from gross photographs of the sacrificed mice at 1 month after intravenous inoculation of ED/Neo (D) or ED/TSLC1 (E) cells. (F) Immunohistochemical staining for TSLC1 protein in liver metastases of the mice inoculated intravenously with ED/TSLC1 cells is shown. An arrow indicates a tumor mass with strong staining with a rabbit anti-TSLC1 antibody; however, the same mass shows no staining with rabbit immunoglobulin (Ig) as a negative control. Magnification, ×100; bars, 400 μm.

TABLE 1. Invasion scores of mice inoculated with ED/Neo or ED/TSLC1 cells

Cell line and mouse	Invasion score for organ by observation:									
	Macroscopic[a]					Microscopic[b]				
	Liver	Kidney	Lung	Ovary	Spleen	Liver	Kidney	Lung	Ovary	Spleen
ED/TSLC1										
T1	3+	−	+/−	1+	−	3+	−	2+	2+	−
T2	3+	−	−	1+	−	3+	−	2+	2+	−
T3	3+	−	+/−	2+	−	3+	−	2+	2+	−
T4	3+	−	−	1+	−	3+	−	2+	2+	−
T5	2+	−	−	2+	−	3+	−	2+	3+	−
T6	3+	−	+/−	1+	−	3+	−	+/−	2+	−
ED/Neo										
N1	−	−	−	2+	−	2+	−	+/−	3+	−
N2	+/−	−	−	1+	−	+/−	−	−	2+	−
N3	−	−	−	2+	−	−	−	+/−	2+	−
N4	−	−	−	1+	−	−	−	−	2+	−
N5	−	−	−	1+	−	ND[c]	ND	ND	ND	ND
N6	−	−	−	1+	−	ND	ND	ND	ND	ND

[a] Subjective invasion scores by macroscopic observation were as follows: −, no invasion; +/−, less than 10% invasion in the organ; 1+, 10 to 30% invasion in the organ; 2+, 30 to 70% invasion in the organ; 3+, over 70% invasion in the organ.
[b] Subjective invasion scores by microscopic observation were as follows: −, no invasion; +/−, less than 1% leukemia cells in the section; 1+, less than 10% leukemia cells in the section; 2+, 10 to 30% leukemia cells in the section; 3+, over 30% leukemia cells in the section
[c] ND, not done.

detected by Western blot analysis (Fig. 1A). Expression of a TSLC1 protein in EL4/TSLC1 cells was also shown on Western blot analysis with KK1, an ATL cell line expressing TSLC1 (12) (Fig. 1B). In an in vitro cell growth assay, 2×10^4 cells were incubated, and their growth was analyzed by direct counting with trypan blue dye staining. EL4 and EL4/TSLC1 cells showed nearly identical proliferation profiles in vitro, while Tax-expressing EL4 cells proliferated more slowly (Fig. 1C). This difference in cell growth might be caused by different expression vectors. In an in vivo growth assay, 2×10^6 cells of each cell line were injected into the peritoneal cavity of C57BL/6J mice: eight mice for EL4 cells as controls, 13 mice for EL4/TSLC1 cells, and eight mice for EL4/GAX cells. All of the mice died of tumor invasion of various organs with ascitic fluids in 40 to 120 days. The median survival time of the control mice injected with EL4 cells or EL4/GAX cells was 72 days. The mice with EL4/TSLC1 cells, however, died within 60 days, with a median survival time of 41 days (Fig. 1D). The phenotypes of the control mice and the EL4/TSLC1 mice were almost identical with invasion of tumors into various organs. Organ metastasis of tumor cells in three EL4/TSLC1-inoculated mice, two EL4-inoculated mice, and one EL4/GAX-inoculated mouse was analyzed and evaluated with hematoxylin-eosin staining. The liver was one of the major sites of metastasis in all three of the EL4/TSLC1-inoculated mice by histopathological analysis but not in the two EL4-inoculated mice or the EL4/GAX-inoculated mouse (Fig. 1E). These results support the role of TSLC1 overexpression in T-lymphoma cells as one of an aggressive factor in the development of leukemia/lymphoma.

In order to investigate the possibility that overexpression of TSLC1 promotes tumor growth and/or infiltration in vivo,

TABLE 2. Clinical characteristics of patients and pathological findings of organ invasion[a]

Patient no.	Age (yr)/sex	Clinical characteristic				Invasion score in NOG mice[b]				TSLC1 expression score[c]
		Diagnosis (ATL type)	WBC (10^9/liter)	Lymphocytes (%)	Atypical cells (%)	Liver	Lung	Spleen	Lymph node	
1	73/M	Chronic	7.8	59	47	3+	3+	3+	ND	3+
2	59/F	Chronic	9.0	75	40	3+	2+	2+	1+	2+
3	66/F	Chronic	29.4	49	75	3+	3+	3+	ND	3+
4	44/F	Chronic	22.6	51	45	3+	2+	2+	2+	2+
5	43/F	Chronic	18.6	63	43	3+	3+	3+	ND	2+
6	54/M	Acute	192.8	65	91	1+	2+	ND	ND	1+
7	58/M	Acute	67.3	71	80	3+	3+	3+	ND	2+
8	65/F	Acute	29.4	25	60	3+	2+	ND	3+	3+
9	68/M	Acute	30.0	79	81	3+	1+	1+	2+	2+
10	66/F	Acute	10.2	38	51	3+	3+	3+	ND	3+

[a] Abbreviations: M, male; F, female; WBC, white blood cells; ND, not done.
[b] Subjective invasion scores were as follows; 0, no invasion; 1+, less than 10% leukemia cells in the section; 2+, 10 to 30% leukemia cells in the section; 3+, over 30% leukemia cells in the section.
[c] Subjective scores of TSLC1 expression in pathological immunostaining were as follows; −, no staining; 1+, faint staining in less than 10% of invasive leukemia cells; 2+, weak to moderate staining in 30 to 70% of invasive leukemia cells; 3+, intense staining in more than 70% of invasive leukemia cells.

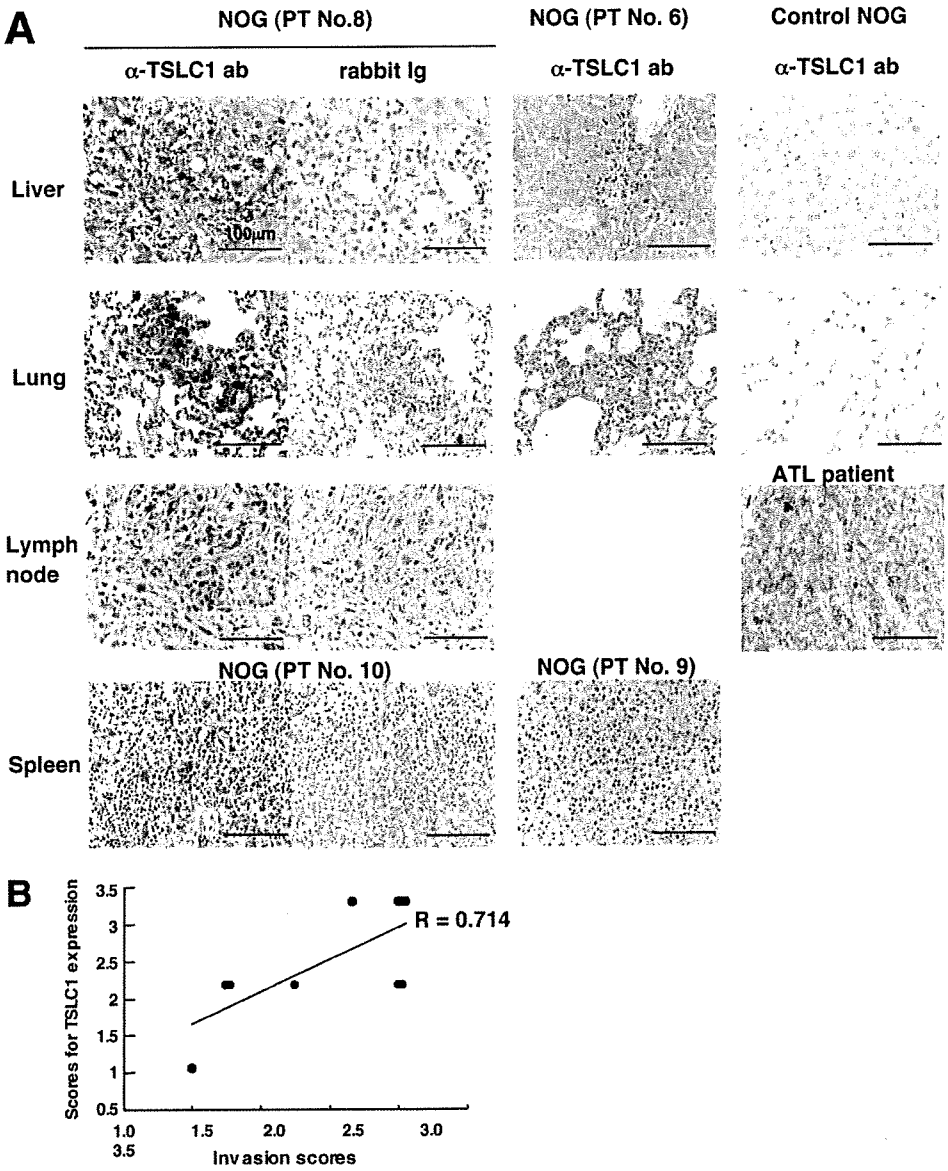

FIG. 3. Growth and infiltration of primary ATL cells in various organs of NOG mice based on TSLC1 expression. (A) Immunohistochemical staining of various organs of NOG mice inoculated with leukemia cells from patient 6, 8, 9, or 10 is shown with the use of rabbit anti-TSLC1 antibody or rabbit immunoglobulin (Ig) as a negative control. Sections from patients 8 and 10 showed severe invasion (invasion score, 3) and dense staining for TSLC1 (expression score, 3), while sections from patients 6 and 9 showed mild invasion (invasion score, 1) and light staining for TSLC1 (expression score, 1). Liver and lung sections from control NOG mice were used as negative controls, and a lymph node from an ATL patient was used as a positive control. Magnification, ×400; bars, 100 μm. (B) The diagram of dispersion between mean values of each invasion score and scores for TSLC1 expression in each NOG mouse inoculated with primary ATL cells showed moderate correlation (R = 0.714).

ATL-derived ED-40515(−) cells (10) were injected into NOG mice. Since expression of TSLC1 in ED-40515(−) cells is severely reduced by promoter methylation, they were transfected with either a TSLC1 expression plasmid (pcDNA3/TSLC1) or a mock plasmid (pcDNA3/Neo). ED/TSLC1 and ED/Neo cells were identified by selection with G-418. High levels of TSLC1 expression were verified in the ED/TSLC1 cells, but not in the ED/Neo cells, by Western blot analysis (Fig. 2A). The ED/TSLC1, ED/Neo, and ED-40515(−) cell lines all showed the same proliferation profile in vitro (Fig. 2B). Cells (10×10^6) were inoculated subcutaneously into the postauricular region of NOG mice, which permitted the observation of tumor growth macroscopically and the measurement of tumor size over a relatively short time (3). The ED/TSLC1 cell lines caused greater formation of larger tumors than did the ED/Neo and ED-40515(−) cell lines (Fig. 2C). The development of clinical signs of near-death (e.g., piloerection, weight loss, and cachexia) in mice at the time of killing was also more prevalent with the ED/TSLC1 cell line. These results suggest that TSLC1 expression in ATL cells enhances in vivo tumor growth in NOG mice.

Since the mice died within 4 weeks after subcutaneous in-

oculation of leukemia cells due to heavy tumor burden, 2×10^6 ED/TSLC1 or ED/Neo cells were intravenously injected into six NOG mice in order to investigate their capacity for invasion of various organs. After 1 month, we sacrificed the mice to determine the extent of organ invasion. Macroscopically, all of the mice injected with ED/TSLC1 cells (six/six) showed severe liver invasion with swelling of the ovaries. None of the mice injected with ED/Neo cells showed liver invasion, but they did show ovarian involvement (Fig. 2D and E). Microscopically, all of the mice inoculated with ED/TSLC1 cells showed severe and massive liver and lung invasions. On the other hand, only one of six mice inoculated with ED/Neo cells showed a large amount of liver metastasis (Table 1). TSLC1 expression in tumor cells infiltrating the liver was confirmed by immunohistochemical staining (Fig. 2F). Thus, overexpression of TSLC1 in ATL cells might enhance organ invasion, and particularly invasion of the liver and lung.

Next, we examined whether primary ATL cells with various levels of expression of TSLC1 could efficiently grow and infiltrate various organs in NOG mice. TSLC1-positive primary ATL cells (2×10^7) from five acute-type and five chronic-type ATL patients were inoculated subcutaneously into the postauricular region of NOG mice (Table 2). All of the mice developed clinical signs of near-death (e.g., piloerection, weight loss, and cachexia) 6 to 8 weeks after inoculation, in addition to the enlargement of the lymph nodes, spleen, lungs, and liver. Microscopically, ATL cells invaded various organs of all ATL-bearing NOG mice to different degrees. Based on results of immunohistochemical staining for TSLC1, all invading leukemia cells expressed TSLC1 protein, compared with no TSLC1 expression in these organs in control NOG mice (Table 2 and Fig. 3A). The dispersion diagram for the levels of invasion and the levels of TSLC1 expression in the leukemia cells showed a correlation coefficient of 0.714, suggesting that there was a moderate correlation between invasive capability and the level of TSLC1 expression (Fig. 3B). Thus, TSLC1 could aid in the formation of a rapidly growing large tumor and massive infiltration of ATL cells into various organs in NOG mice. Since TSLC1 is expressed in various types of ATL cells, including smoldering and chronic types, it might be a promising target for the development of a new anti-ATL therapy. The NOG mouse model system described in the present study could provide a novel means by which to understand and investigate the further importance of TSLC1 in ATL progression.

We thank S. Ichinose of the Instrumental Analysis Research Center; S. Endo of the Animal Research Center, Tokyo Medical and Dental University; and Y. Sato of the National Institute of Infectious Diseases for her excellent technical assistance. Anti-Tax (MI73) antibody was the kind gift of Y. Namba and M. Matsuoka (Institute for Virus Research, Kyoto University).

Supported by grants from the Ministry of Education, Science, and Culture; the Ministry of Health, Labor, and Welfare; and Human Health Science of Japan.

REFERENCES

1. **Ballard, D. W., E. Bohnlein, J. W. Lowenthal, Y. Wano, B. R. Franza, and W. C. Greene.** 1988. HTLV-I tax induces cellular proteins that activate the B element in the IL-2 receptor gene. Science **241**:1652–1655.
2. **Cross, S. L., M. B. Feinberg, J. B. Wolf, N. J. Holbrook, F. Wong-Staal, and W. J. Leonard.** 1987. Regulation of the human interleukin-2 receptor chain promoter: activation of a nonfunctional promoter by the transactivator gene of HTLV-I. Cell **49**:47–56.
3. **Dewan, M. Z., K. Terashima, M. Taruishi, H. Hasegawa, M. Ito, Y. Tanaka, N. Mori, T. Sata, Y. Koyanagi, M. Maeda, Y. Kubuki, A. Okayama, M. Fujii, and N. Yamamoto.** 2003. Rapid tumor formation of human T-cell leukemia virus type 1-infected cell lines in novel NOD-SCID/cγ^{null} mice: suppression by an inhibitor against NF-κB. J. Virol. **77**:5286–5294.
4. **Dewan, M. Z., J. N. Uchihara, K. Terashima, M. Honda, T. Sata, M. Ito, N. Fujii, K. Uozumi, K. Tsukasaki, M. Tomonaga, Y. Kubuki, A. Okayama, M. Toi, N. Mori, and N. Yamamoto.** 2006. Efficient intervention of growth and infiltration of primary adult T-cell leukemia cells by an HIV protease inhibitor, ritonavir. Blood **107**:716–724.
5. **Felber, B. K., H. Paskalis, C. Kleinman-Ewing, F. Wong-Staal, and G. N. Pavlakis.** 1985. The pX protein of HTLV-I is a transcriptional activator of its long terminal repeats. Science **229**:675–679.
6. **Furuta, R. A., K. Sugiura, S. Kawakita, T. Inada, S. Ikehara, T. Matsuda, and J. Fujisawa.** 2002. Mouse model for the equilibration interaction between the host immune system and human T-cell leukemia virus type 1 gene expression. J. Virol. **76**:2703–2713.
7. **Hinuma, Y., K. Nagata, M. Hanaoka, M. Nakai, T. Matsumoto, K. I. Kinoshita, S. Shirakawa, and I. Miyoshi.** 1981. Adult T-cell leukemia: antigen in an ATL cell line and detection of antibodies to the antigen in human sera. Proc. Natl. Acad. Sci. USA **78**:6476–6480.
8. **Ito, M., H. Hiramatsu, K. Kobayashi, K. Suzue, M. Kawahata, K. Hioki, Y. Ueyama, Y. Koyanagi, K. Sugamura, K. Tsuji, T. Heike, and T. Nakahata.** 2002. NOD/SCID/.cnull mouse: an excellent recipient mouse model for engraftment of human cells. Blood **100**:3175–3182.
9. **Kuramochi, M., H. Fukuhara, T. Nobukuni, T. Kanbe, T. Maruyama, H. P. Ghosh, M. Pletcher, M. Isomura, M. Onizuka, T. Kitamura, T. Sekiya, R. H. Reeves, and Y. Murakami.** 2001. TSLC1 is a tumor suppressor gene in human non-small cell lung cancer. Nat. Genet. **27**:427–730.
10. **Maeda, M., A. Shimizu, K. Ikuta, H. Okamoto, M. Kashihara, T. Uchiyama, T. Honjo, and J. Yodoi.** 1985. Origin of human T-lymphotrophic virus I-positive T cell lines in adult T cell leukemia. Analysis of T cell receptor gene rearrangement. J. Exp. Med. **162**:2169–2174.
11. **Maruyama, M., H. Shibuya, H. Harada, M. Hatakeyama, M. Seiki, T. Fujita, J. Inoue, M. Yoshida, and T. Taniguchi.** 1987. Evidence for aberrant activation of the interleukin-2 autocrine loop by HTLV-1-encoded p40x and T3/Ti complex triggering. Cell **48**:343–350.
12. **Masuda, M., M. Yagita, H. Fukuhara, M. Kuramochi, T. Maruyama, A. Nomoto, and Y. Murakami.** 2002. The tumor suppressor protein TSLC1 is involved in cell-cell adhesion J. Biol. Chem. **277**:31014–31019.
13. **Murakami, Y., T. Nobukuni, K. Tamura, T. Maruyama, T. Sekiya, Y. Arai, H. Gomyou, A. Tanigami, M. Ohki, D. Cabin, P. Frischmeyer, P. Hunt, and R. H. Reeves.** 1998. Localization of tumor suppressor activity important in non-small cell lung carcinoma on chromosome 11q. Proc. Natl. Acad. Sci. USA **95**:8153–8158.
14. **Poiesz, B. J., F. W. Ruscetti, A. F. Gazdar, P. A. Bunn, J. D. Minna, and R. C. Gallo.** 1980. Detection and isolation of type C retrovirus particles from fresh and cultured lymphocytes of a patient with cutaneous T-cell lymphoma. Proc. Natl. Acad. Sci. USA **77**:7415–7419.
15. **Sasaki, H., I. Nishikata, T. Shiraga, E. Akamatsu, T. Fukami, T. Hidaka, Y. Kubuki, A. Okayama, K. Hamada, H. Okabe, Y. Murakami, H. Tsubouchi, and K. Morishita.** 2005. Overexpression of a cell adhesion molecule, TSLC1, as a possible molecular marker for acute type of adult T-cell leukemia. Blood **105**:1204–1213.
16. **Sodroski, J. G., C. A. Rosen, and W. A. Haseltine.** 1984. Transacting transcriptional activation of the long terminal repeat of human T lymphotropic viruses in infected cells. Science **225**:381–385.
17. **Yamaguchi, K., and T. Watanabe.** 2002. Human T lymphotropic virus type-I and adult T-cell leukemia in Japan. Int. J. Hematol. **76**:240–245.
18. **Yoshida, M., I. Miyoshi, and Y. Hinuma.** 1982. Isolation and characterization of retrovirus from cell lines of human adult T-cell leukemia and its implication in the disease. Proc. Natl. Acad. Sci. USA **79**:2031–2035.

nature

Vol 456|13 November 2008|doi:10.1038/nature07383

LETTERS

Loss of the autophagy protein Atg16L1 enhances endotoxin-induced IL-1β production

Tatsuya Saitoh[1,3]*, Naonobu Fujita[4]*, Myoung Ho Jang[2], Satoshi Uematsu[1,3], Bo-Gie Yang[1,3], Takashi Satoh[1,3], Hiroko Omori[4], Takeshi Noda[4], Naoki Yamamoto[5], Masaaki Komatsu[6,7,8], Keiji Tanaka[6], Taro Kawai[1,3], Tohru Tsujimura[9], Osamu Takeuchi[1,3], Tamotsu Yoshimori[4,10] & Shizuo Akira[1,3]

Systems for protein degradation are essential for tight control of the inflammatory immune response[1,2]. Autophagy, a bulk degradation system that delivers cytoplasmic constituents into autolysosomes, controls degradation of long-lived proteins, insoluble protein aggregates and invading microbes, and is suggested to be involved in the regulation of inflammation[3–5]. However, the mechanism underlying the regulation of inflammatory response by autophagy is poorly understood. Here we show that Atg16L1 (autophagy-related 16-like 1), which is implicated in Crohn's disease[6,7], regulates endotoxin-induced inflammasome activation in mice. Atg16L1-deficiency disrupts the recruitment of the Atg12-Atg5 conjugate to the isolation membrane, resulting in a loss of microtubule-associated protein 1 light chain 3 (LC3) conjugation to phosphatidylethanolamine. Consequently, both autophagosome formation and degradation of long-lived proteins are severely impaired in Atg16L1-deficient cells. Following stimulation with lipopolysaccharide, a ligand for Toll-like receptor 4 (refs 8, 9), Atg16L1-deficient macrophages produce high amounts of the inflammatory cytokines IL-1β and IL-18. In lipopolysaccharide-stimulated macrophages, Atg16L1-deficiency causes Toll/IL-1 receptor domain-containing adaptor inducing IFN-β (TRIF)-dependent activation of caspase-1, leading to increased production of IL-1β. Mice lacking Atg16L1 in haematopoietic cells are highly susceptible to dextran sulphate sodium-induced acute colitis, which is alleviated by injection of anti-IL-1β and IL-18 antibodies, indicating the importance of Atg16L1 in the suppression of intestinal inflammation. These results demonstrate that Atg16L1 is an essential component of the autophagic machinery responsible for control of the endotoxin-induced inflammatory immune response.

Autophagy is a bulk degradation system, which controls the clearance and re-use of intracellular constituents, and is important for the maintenance of an amino acid pool essential for survival[3–5]. In addition, recent studies have disclosed multiple roles of autophagy in the regulation of cell death, differentiation and anti-microbial response in mammals[4,5]. Yeast genetic screening studies have identified a variety of essential components of autophagic machinery, called Atg proteins, which are phylogenetically highly conserved, and several mammalian counterparts, such as Atg5 and Atg7, have been reported[3–5]. Previously, we systematically characterized mammalian homologues of Atg proteins and identified Atg16L1 protein as an Atg5-binding protein[10]. Its coiled-coil domain, which mediates self-multimerization, is essentially required for starvation-induced autophagy in yeast, and this domain is conserved in mammalian Atg16L1 (refs 3, 10; Fig. 1a). We have proposed that the coiled-coil domain of Atg16L1 is required for the formation of an ~800 kDa high molecular weight protein complex with the Atg12-Atg5 conjugate and defines the site where LC3 (homologue of yeast Atg8) is conjugated to phosphatidylethanolamine (PE), an essential process for autophagy, by recruitment of an Atg3-LC3 intermediate to a source membrane of an autophagosome[10,11]. In addition, Atg16L1 has seven WD40 repeats at the carboxy terminus, which are absent in yeast Atg16 (ref. 10). Recent genome-wide association studies identified Atg16L1 as a candidate gene responsible for susceptibility to Crohn's disease[6,7]. However, the importance of Atg16L1 in autophagy and its role in inflammation have not been fully understood. Hence, we generated Atg16L1 mutant mice and examined the function of Atg16L1 in autophagosome formation as well as in the regulation of immune responses.

Atg16L1 mutant mice express deleted forms of Atg16L1 protein lacking the entire coiled-coil domain (Fig. 1a, b, and Supplementary Fig. 1a–c). However, such aberrant proteins do not act as dominant-negative molecules, because ectopic expression of truncated Atg16L1 protein lacking the coiled-coil domain (ΔCCD) in wild-type mouse embryonic fibroblasts (MEFs) did not interfere with autophagy (Supplementary Fig. 2a, b). Most Atg16L1-deficient mice died within 1 day of delivery, indicating that Atg16L1 is required for survival during neonatal starvation (Supplementary Fig. 1d, e). This phenotype is similar to that observed in Atg5- or Atg7-deficient mice[12,13]. Although Atg16L1 associates with Atg12-Atg5, Atg16L1 was dispensable for Atg12 conjugation to Atg5 (Fig. 1b). On the other hand, Atg16L1 was required for LC3 conjugation to PE (Fig. 1b). In Atg16L1-deficient MEFs, formation of the high molecular weight protein complex was disrupted and Atg12-Atg5 puncta were hardly observed (Fig. 1c, d, and Supplementary Fig. 3, 4a). On the other hand, GFP-Atg5 free from Atg12-conjugation formed puncta in Atg7-deficient MEFs or Atg5-deficient MEFs complemented with GFP-Atg5^{K130R}, although these puncta did not colocalize with LC3 (Fig. 1c, d, Supplementary Figs 4b, 5, data not shown). Formation of autophagosomes under the starved condition was not observed in Atg16L1-deficient MEFs, resulting in a decrease in the bulk degradation of long-lived proteins and the accumulation of p62/SQSTM1 (Fig. 1b–f). These results indicated that Atg16L1 is essentially required for autophagy by regulating the localization of the Atg12-Atg5 conjugate.

[1]Laboratory of Host Defense, [2]Laboratory of Gastrointestinal Immunology, WPI Immunology Frontier Research Center, Osaka University, 3-1 Yamada-oka, Suita, Osaka 565-0871, Japan. [3]Department of Host Defense, [4]Department of Cellular Regulation, Research Institute for Microbial Diseases, Osaka University, 3-1 Yamada-oka, Suita, Osaka 565-0871, Japan. [5]AIDS Research Center, National Institute of Infectious Diseases, Toyama 1-23-1, Shinjuku-ku, Tokyo 162-8640, Japan. [6]Laboratory of Frontier Science, Tokyo Metropolitan Institute of Medical Science, Bunkyo-ku, Tokyo 113-8613, Japan. [7]Department of Biochemistry, Juntendo University School of Medicine, 2-1-1 Hongo Bunkyo-ku, Tokyo 113-8421, Japan. [8]PRESTO, Japan Science and Technology Corporation, Kawaguchi, Saitama 332-0012, Japan. [9]Department of Pathology, Hyogo College of Medicine, 1-1 Mukogawa-cho, Nishinomiya, Hyogo 663-8501, Japan. [10]CREST, Japan Science and Technology Agency, 4-1-8 Honcho, Kawaguchi, Saitama 332-0012, Japan.
*These authors contributed equally to this work.

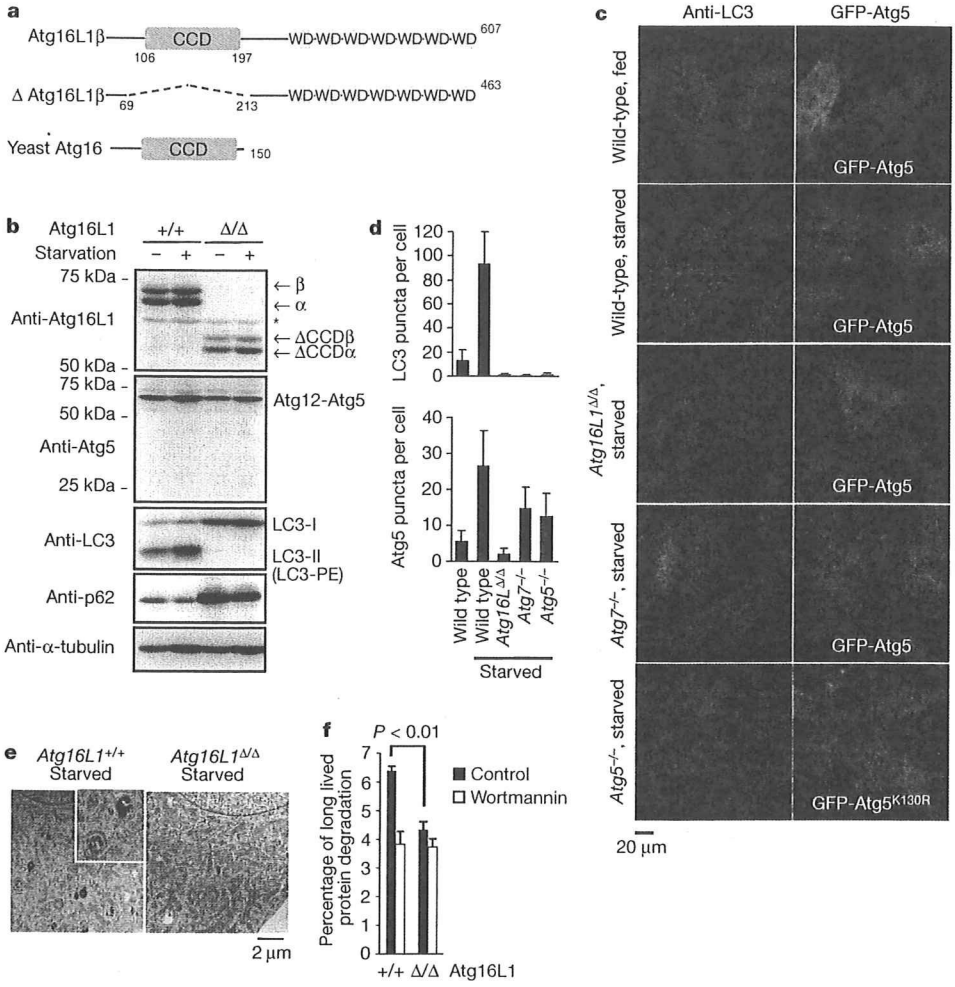

Figure 1 | Atg16L1 is essential for autophagy. **a**, Schematic structure of wild-type or truncated (Δ) Atg16L1 protein. CCD, Coiled-coil domain; WD, WD40 domain. Here and below, suffix α or β indicates isoform α or β. **b–d**, MEFs were cultured in nutrient-rich medium (fed) or Hanks' buffer (starved) for 1 h. Total cell lysates were prepared, and blotted with the indicated antibodies (**b**). α, β, indicate Atg16L1 isoform α, β; ΔCCD indicates Atg16L1ΔCCD; asterisk indicates a non-specific band. *Atg16L1*$^{\Delta/\Delta}$ indicates mice expressing ΔAtg16L1. The number of endogenous LC3 or GFP-Atg5 dots was counted (**c, d**). The results shown are mean + s.d. ($n > 20$). **e**, Electron micrograph of starved MEFs. **f**, Degradation of long-lived proteins in MEFs. Wortmannin is an autophagy inhibitor. The results shown are mean + s.d. Statistical significance (*P* value) was determined by the Student's *t*-test.

Although the involvement of autophagic machinery in the Toll-like receptor (TLR)-mediated antiviral response and phagocytosis have been reported[14,15], it is still unclear whether autophagy controls TLR-mediated inflammatory responses. We examined the role of Atg16L1 in the production of inflammatory cytokines, such as TNFα, IL-6 and IL-1β, in response to lipopolysaccharide (LPS), a major component of bacterial endotoxin[8]. Although both messenger RNA expression and production of TNFα, IL-6 and IFN-β were almost normal in Atg16L1-deficient fetal liver-derived macrophages, IL-1β production was highly elevated compared with that in wild-type macrophages (Fig. 2a, Supplementary Fig. 6). IL-1β mRNA synthesis was not impaired in Atg16L1-deficient macrophages, indicating that IL-1β production is enhanced at the post-transcriptional level in Atg16L1-deficient macrophages (Supplementary Fig. 6). Synthetic lipid A, an active component of LPS, also potently induced IL-1β production in Atg16L1-deficient cells (Fig. 2b). On the other hand, ectopic expression of the Atg16L1 protein lacking coiled-coil domain (ΔCCD) in RAW264.7 cells did not affect LPS-induced IL-1β production (Supplementary Fig. 2c, d). These results indicated that Atg16L1-deficiency is responsible for the elevated production of IL-1β.

We next generated chimaeric mice by transplantation of fetal liver cells into lethally irradiated CD45.1 mice to examine IL-1β production in other types of macrophage (Supplementary Fig. 7a–c). Following stimulation with LPS, peritoneal and bone-marrow macrophages deficient in Atg16L1 showed enhanced IL-1β production compared with wild-type macrophages (Supplementary Fig. 7d, e). Non-invasive Gram-negative bacteria, such as *Escherichia coli, Enterobacter aerogenes* and *Klebsiella pneumonia*, which are habitants in the commensal flora, also potently induced IL-1β production in Atg16L1-deficient cells (Supplementary Fig. 8a). On the other hand, the production of IL-1β and apoptosis induced by *Salmonella typhimurium*, an invasive Gram-negative bacterium, is almost normal in Atg16L1-deficient macrophages (Fig. 2c, Supplementary Fig. 9c). We also found that Atg16L1-deficient macrophages produced a high amount of IL-1β following stimulation by ATP or monosodium urate (MSU), an activator of the Nalp3 inflammasome[16,17] (Fig. 2c). Atg16L1-deficient macrophages normally produced inflammatory cytokine in response to muramyldipeptide, a ligand for NOD2 (ref. 16), indicating that Atg16L1 is not involved in signalling downstream of NOD2, whose de-regulation is also implicated in Crohn's disease[16] (Supplementary Fig. 10).

The expression levels of immature IL-1β protein following LPS stimulation in Atg16L1-deficient macrophages were almost comparable to those in wild-type cells, indicating an abnormality of post-translational regulation (Fig. 2d). Cleaved caspase-1, an activated

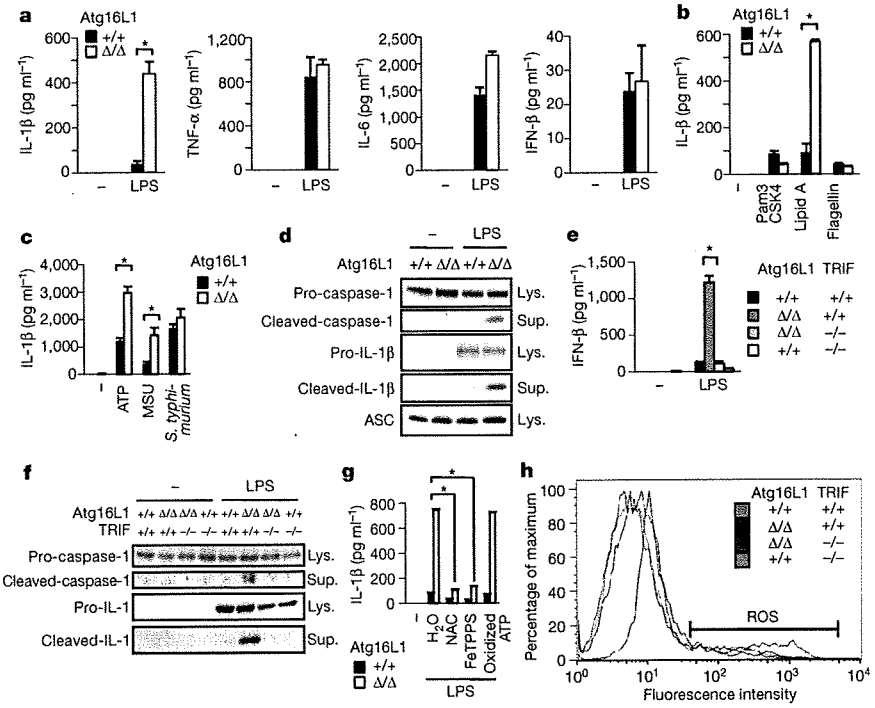

Figure 2 | Elevated endotoxin-induced IL-1β production from Atg16L1-deficient macrophages. **a**, Cytokine production from macrophages stimulated with LPS (100 ng ml^{-1}) for 24 h. Statistical significance was determined by the Student's *t*-test. $*P < 0.01$. **b**, IL-1β production from macrophages stimulated with indicated ligands. **c**, IL-1β production from LPS-primed macrophages infected with *S. typhimurium* (multiplicity of infection, m.o.i., 1), or stimulated with ATP or MSU for 1 h. **d**, Expression levels of caspase-1 and IL-1β in macrophages. Lys., cell lysates; Sup., culture supernatants. **e**, LPS-induced production of IL-1β from macrophages with the indicated phenotype. **f**, Expression levels of caspase-1 and IL-1β in macrophages treated as in **e**. **g**, Effect of the ROS scavenger FeTPPS (25 μM), N-acetyl-L-cysteine (NAC; 25 mM) or P2X7 receptor antagonist oxidized ATP (250 μM) on IL-1β production. **h**, ROS in LPS-stimulated macrophages were detected by CM-H_2DCFDA staining.

form that mediates processing of IL-1β and apoptosis[16,17], was detected in the culture supernatants of Atg16L1-deficient macrophages following LPS stimulation, and was responsible for the production of IL-1β and the induction of apoptosis (Fig. 2d, Supplementary Figs 9a, b, 11). IL-18 production, which is regulated by caspase-1-mediated cleavage[17], was also enhanced in response to LPS in Atg16L1-deficient macrophages (Supplementary Fig. 12). Recent studies have disclosed that NF-κB and p38 signalling pathways regulate the activation of caspase-1 and the induction of cell death in macrophages stimulated with LPS[18,19]. However, activation of NF-κB, p38 and IRF-3 signalling pathways by LPS was comparable between wild-type and Atg16L1-deficient macrophages (Supplementary Fig. 13). Among TLR family members, TLR2, TLR4 and TLR5 recognize bacterial components and play important roles in the anti-bacterial response[8]. Importantly, TLR4 ligand, but not ligands for TLR2 or TLR5, induced potent IL-1β production from Atg16L1-deficient macrophages (Fig. 2b, Supplementary Fig. 14). Enhancement of IL-1β production in Atg16L1-deficient macrophages was also induced by ligands for the viral nucleotide-sensing TLRs, TLR3, TLR7 and TLR9, although the production induced by these ligands was lower than that induced by LPS (Supplementary Fig. 14).

These findings prompted us to assess the involvement of the TRIF/IFN signalling, which is strongly triggered by the engagement of TLR4 in macrophages[8] and regulates apoptosis[18]. Consistent with this hypothesis, Atg16L1/TRIF double-deficient macrophages failed

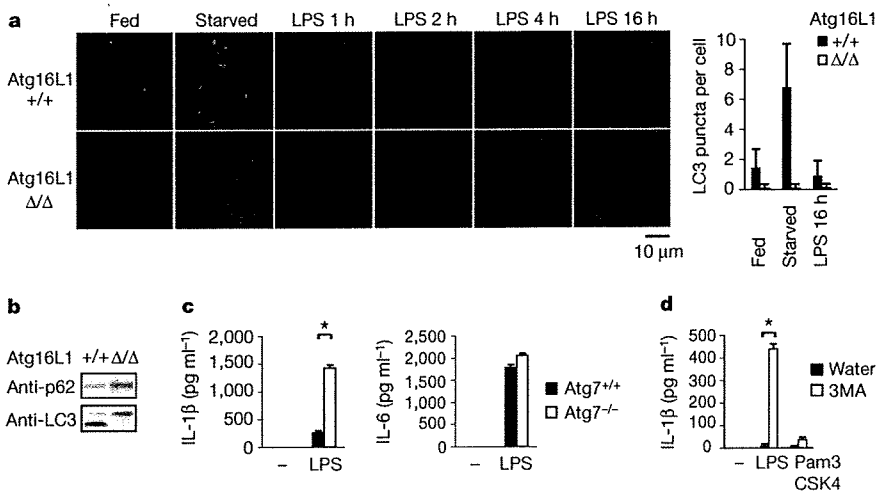

Figure 3 | Disruption of basal autophagy enhances LPS-induced IL-1β production. **a**, Macrophages were stimulated with LPS (100 ng ml^{-1}) for the indicated time period. The number of endogenous LC3 dots within each cell was counted. The results shown are mean + s.d. ($n > 100$). **b**, Expression levels of p62 and LC3 in macrophages. **c**, IL-1β and IL-6 production by wild-type or Atg7-deficient macrophages stimulated with LPS. Statistical significance was determined by the Student's *t*-test. $*P < 0.01$. **d**, Macrophages were pre-treated with or without 10 mM 3MA and then stimulated with the indicated ligands.

to produce IL-1β due to a lack of caspase-1 activation in response to LPS (Fig. 2e, f). The simultaneous stimulation of Atg16L1-deficient macrophages with IFN-β or IFN-γ enhanced IL-1β production and apoptosis induced by TLR2 ligand (Supplementary Figs 9d, 15a). Recent studies have disclosed that K^+-efflux and reactive oxygen species (ROS), especially peroxynitrate, play important roles in the production of IL-1β induced by ATP, MSU and asbestos[16,17,20,21]. Similarly, the enhanced IL-1β production from Atg16L1-deficient macrophages required K^+-efflux and ROS generation (Fig. 2g, Supplementary Figs 15b, 16). The level of ROS in Atg16L1-deficient macrophages was higher than that in Atg16L1/TRIF double-deficient or wild-type macrophages following LPS stimulation (Fig. 2h). Oxidized ATP, an antagonist for the P2X7 receptor, did not inhibit LPS-induced IL-1β production, indicating that extracellular ATP is not involved in its production (Fig. 2g). These results indicate that loss of Atg16L1 in macrophages causes aberrant LPS-induced IL-1β production in a TRIF-dependent manner. ROS might be accumulated in Atg16L1-deficient macrophages undergoing apoptosis and trigger caspase-1 activation following LPS stimulation.

The involvement of TLR signalling in the induction of autophagy has been recently reported[22,23]. Therefore we examined if stimulation of TLR4 or other TLRs induces puncta formation by endogenous LC3. In contrast to previous reports, LPS stimulation did not increase the number of LC3 puncta in primary macrophages, although nutrient deprivation induced the formation of autophagosomes (Fig. 3a, Supplementary Fig. 17a–c). Stimulation by other ligands for TLRs also failed to increase the number of puncta of endogenous LC3 in these macrophages (Supplementary Fig. 17b, d, e). Co-incubation with non-invasive bacteria did not increase the number of autophagosomes in macrophages (Supplementary Fig. 8b). On the other hand, infection with *S. typhimurium* resulted in Atg16L1-dependent formation of bacteria autophagosomes, even in the absence of both MyD88 and TRIF, essential adaptor molecules for TLR signalling pathways[8,9] (Supplementary Fig. 18a, b). These results indicated that TLR signalling is not associated with the formation of autophagosomes in primary macrophages.

Increasing evidence has revealed that basal autophagy plays critical roles under both physiological and pathological conditions, including neurodegeneration, hepatic dysfunction and the immune response[13,24–26]. In Atg16L1-deficient macrophages, autophagosomes were hardly detected and p62/SQSTM1 protein was accumulated under nutrient-rich conditions, indicating that basal autophagy is almost completely inhibited (Fig. 3a, b). Atg7-deficient macrophages also produced high levels of IL-1β in response to LPS, but produced normal levels of IL-6 (Fig. 3c). A chemical inhibitor of autophagy, 3-methyladenine (3MA), significantly enhanced production of IL-1β from wild-type peritoneal macrophages induced by stimulation with LPS, but not with ligand for TLR2 (Fig. 3d). Macrophages treated with 3MA underwent apoptosis following LPS stimulation (Supplementary Fig. 9e). Further, transient expression of inactive mutant of Atg4B, which inhibits the LC3 lipidation, enhanced LPS-induced IL-1β production in RAW264.7 cells (Supplementary Fig. 19a, b). These results indicate that inhibition of basal autophagy induces IL-1β overproduction.

Aberrant expression of inflammatory cytokines, including IL-1β and IL-18, has been shown to be involved in the development of colitis[27,28], and recent studies have reported that Atg16L1 is a candidate susceptibility gene for Crohn's disease[6,7]. Under specific pathogen-free conditions, Atg16L1-deficient chimaeric mice did not develop spontaneous colitis, and the colons of newborn Atg16L1-deficient mice were not inflamed (Supplementary Fig. 20a, b). The number of bacteria in the faeces of wild-type or Atg16L1-deficient chimaeric mice was almost same, and no bacteria were detected in spleen (Supplementary Fig. 20c, d). The number of $CD4^+Foxp3^+$ regulatory T cells, which suppress the inflammatory response and are required for immune homeostasis[29], was almost normal in the spleens and mesenteric lymph nodes of Atg16L1-deficient chimaeric mice (Supplementary Fig. 21a, b). We next assessed if Atg16L1-deficiency exacerbates inflammation in a dextran sulphate sodium (DSS)-induced experimental model of colitis. Strikingly, all chimaeric mice with Atg16L1-deficient haematopoietic cells died together with severe body weight loss following seven days of DSS exposure, whereas all chimaeric mice expressing wild-type Atg16L1 survived (Fig. 4a, b). Histological analyses revealed much severer inflammation in the distal colons of Atg16L1-deficient mice than in wild-type controls, with larger areas of ulceration and increased infiltration of lymphocytes

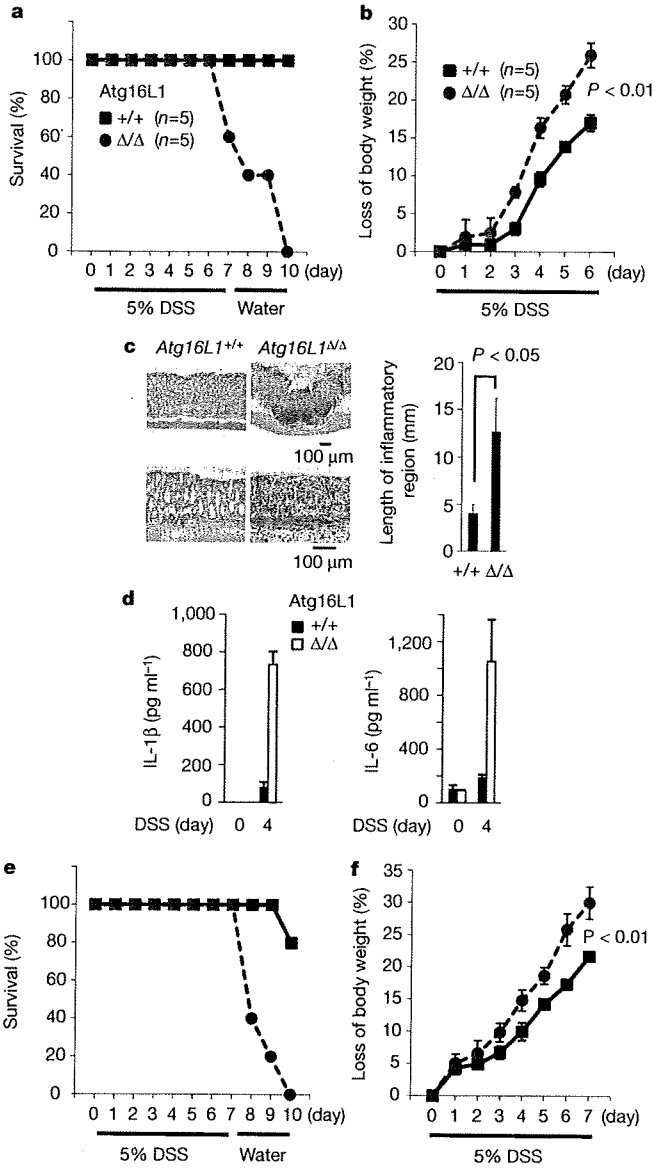

Figure 4 | Severe DSS-induced colitis in Atg16L1-deficient chimaeric mice. **a**, **b**, Fetal liver chimaeric mice were given 5% DSS in drinking water for 7 days. The survival (**a**) and weight loss (**b**) of each mouse genotype were plotted. The results shown are mean ± s.d. Statistical significance was determined by the Student's *t*-test. **c**, Typical distal colon appearance 6 days after the initiation of DSS administration. The results shown are mean ± s.d. ($n = 3$, each group). **d**, Expression levels of IL-1β and IL-18 in serum ($n = 5$, each group). **e**, **f**, Atg16L1-deficient chimaeric mice given 5% DSS in drinking water were intraperitoneally injected with both anti-IL-1β and anti-IL-18 neutralizing antibodies (squares; $n = 5$) or isotype control IgG (circles; $n = 5$) at days 1, 3, 5 and 7. The survival (**e**) and weight loss (**f**) of each mouse genotype were plotted.

(Fig. 4c). The levels of the proinflammatory cytokines IL-1β and IL-18 were significantly elevated in the sera of DSS-treated Atg16L1-deficient chimaeric mice relative to the levels in wild-type counterparts (Fig. 4d). Mortality and loss of body weight after DSS-exposure in Atg16L1-deficient chimaeric mice were improved by the injection of neutralizing antibodies for IL-1β and IL-18, showing the involvement of excessive production of these cytokines in the development of severe colitis (Fig. 4e, f). Administration of 3MA increased the level of IL-1β in serum and worsened the survival rate of mice treated with DSS, suggesting that autophagy protects mice from massive inflammation during colitis (Supplementary Fig. 22).

Our present study highlights a novel role for autophagy in the regulation of the inflammatory immune response. Autophagy controls inflammasome activation and limits production of the inflammatory cytokines IL-1β and IL-18. Given the importance of elevated expression of IL-1β and IL-18 caused by Atg16L1 deficiency in the pathology of chemical-induced colitis, it would be of interest to examine the involvement of autophagy in the pathogenesis of inflammatory bowel diseases such as Crohn's disease.

METHODS SUMMARY

Mice, reagents, cells and plasmids. Details are given in Methods.

Preparation of macrophages. E15.5 fetal liver stem cells from wild-type or Atg16L1-deficient littermates were cultured in the presence of GM-CSF (10 ng ml^{-1}) for 7 days to generate fetal liver macrophages. Unattached cells were removed on days 2, 4 and 6. Unless otherwise noted, fetal liver macrophages were used in the experiments. Bone-marrow-derived and peritoneal macrophages were prepared as described[9].

Histopathological analysis. The colon was removed and fixed with 4% PFA. The paraffin sections were stained with haematoxylin and eosin (H&E), and histologically analysed.

RT–PCR, immunoblotting, ELISA. Details of RT–PCR procedures are given in Methods. Immunoblotting was performed as described[11], and the experiments were repeated at least twice. The level of cytokine production was measured by ELISA according to the manufacturer's instructions. The results shown are means ± s.d. from three separate samples. The experiments were repeated at least three times.

Fluorescence microscopy analysis. Cells cultured on coverslips were fixed with 3% paraformaldehyde, and subjected to immunocytochemistry[11]. Samples were examined under a fluorescence laser scanning confocal FV1000 microscope (Olympus).

Detection of ROS. Macrophages were stimulated with LPS for 22 h, and then stained with CM-H_2DCFDA (10 μM; Molecular Probes), a fluorescent indicator for ROS, for 2 h. The level of fluorescence was determined by flow cytometry. The experiments were repeated at least three times.

Gel filtration, electron microscopy analysis, bulk protein degradation assay. Gel filtration analysis was performed as described[11]; electron microscopy analysis was performed as described[30]; details on the bulk protein degradation assay are given in Methods.

Full Methods and any associated references are available in the online version of the paper at www.nature.com/nature.

Received 7 August; accepted 26 August 2008.
Published online 5 October 2008.

1. Liu, Y. C., Penninger, J. & Karin, M. Immunity by ubiquitylation: A reversible process of modification. *Nature Rev. Immunol.* 5, 941–952 (2005).
2. Wang, Y. *et al.* Lysosome-associated small Rab GTPase Rab7b negatively regulates TLR4 signaling in macrophages by promoting lysosomal degradation of TLR4. *Blood* 110, 962–971 (2007).
3. Ohsumi, Y. Molecular dissection of autophagy: Two ubiquitin-like systems. *Nature Rev. Mol. Cell Biol.* 2, 211–216 (2001).
4. Mizushima, N., Levine, B., Cuervo, A. M. & Klionsky, D. J. Autophagy fights disease through cellular self-digestion. *Nature* 451, 1069–1075 (2008).
5. Levine, B. & Deretic, V. Unveiling the roles of autophagy in innate and adaptive immunity. *Nature Rev. Immunol.* 7, 767–777 (2007).
6. Hampe, J. *et al.* A genome-wide association scan of nonsynonymous SNPs identifies a susceptibility variant for Crohn disease in ATG16L1. *Nature Genet.* 39, 207–211 (2007).
7. Rioux, J. D. *et al.* Genome-wide association study identifies new susceptibility loci for Crohn disease and implicates autophagy in disease pathogenesis. *Nature Genet.* 39, 596–604 (2007).
8. Akira, S., Uematsu, S. & Takeuchi, O. Pathogen recognition and innate immunity. *Cell* 124, 783–801 (2006).
9. Yamamoto, M. *et al.* Role of adaptor TRIF in the MyD88-independent toll-like receptor signaling pathway. *Science* 301, 640–643 (2003).
10. Mizushima, N. *et al.* Mouse Apg16L, a novel WD-repeat protein, targets to the autophagic isolation membrane with the Apg12-Apg5 conjugate. *J. Cell Sci.* 116, 1679–1688 (2003).
11. Fujita, N., Itoh, T., Fukuda, M., Noda, T. & Yoshimori, T. The Atg16L complex specifies the site of LC3 lipidation for membrane biogenesis in autophagy. *Mol. Biol. Cell* 19, 2092–2100 (2008).
12. Kuma, A. *et al.* The role of autophagy during the early neonatal starvation period. *Nature* 432, 1032–1036 (2004).
13. Komatsu, M. *et al.* Impairment of starvation-induced and constitutive autophagy in Atg7-deficient mice. *J. Cell Biol.* 169, 425–434 (2005).
14. Lee, H. K., Lund, J. M., Ramanathan, B., Mizushima, N. & Iwasaki, A. Autophagy-dependent viral recognition by plasmacytoid dendritic cells. *Science* 315, 1398–1401 (2007).
15. Sanjuan, M. A. *et al.* Toll-like receptor signalling in macrophages links the autophagy pathway to phagocytosis. *Nature* 450, 1253–1257 (2007).
16. Kanneganti, T. D., Lamkanfi, M. & Núñez, G. Intracellular NOD-like receptors in host defense and disease. *Immunity* 27, 549–559 (2007).
17. Pétrilli, V., Dostert, C., Muruve, D. A. & Tschopp, J. The inflammasome: A danger sensing complex triggering innate immunity. *Curr. Opin. Immunol.* 19, 615–622 (2007).
18. Hsu, L. C. *et al.* The protein kinase PKR is required for macrophage apoptosis after activation of Toll-like receptor 4. *Nature* 428, 341–345 (2004).
19. Greten, F. R. *et al.* NF-κB is a negative regulator of IL-1β secretion as revealed by genetic and pharmacological inhibition of IKKβ. *Cell* 130, 918–931 (2007).
20. Dostert, C. *et al.* Innate immune activation through Nalp3 inflammasome sensing of asbestos and silica. *Science* 320, 674–677 (2008).
21. Hewinson, J., Moore, S. F., Glover, C., Watts, A. G. & MacKenzie, A. B. A key role for redox signaling in rapid P2X7 receptor-induced IL-1beta processing in human monocytes. *J. Immunol.* 180, 8410–8420 (2008).
22. Xu, Y. *et al.* Toll-like receptor 4 is a sensor for autophagy associated with innate immunity. *Immunity* 27, 135–144 (2007).
23. Delgado, M. A., Elmaoued, R. A., Davis, A. S., Kyei, G. & Deretic, V. Toll-like receptors control autophagy. *EMBO J.* 27, 1110–1121 (2008).
24. Hara, T. *et al.* Suppression of basal autophagy in neural cells causes neurodegenerative disease in mice. *Nature* 441, 885–889 (2006).
25. Komatsu, M. *et al.* Homeostatic levels of p62 control cytoplasmic inclusion body formation in autophagy-deficient mice. *Cell* 131, 1149–1163 (2007).
26. Paludan, C. *et al.* Endogenous MHC class II processing of a viral nuclear antigen after autophagy. *Science* 307, 593–596 (2005).
27. Maeda, S. *et al.* Nod2 mutation in Crohn's disease potentiates NF-κB activity and IL-1β processing. *Science* 307, 737–738 (2005).
28. Ishikura, T. *et al.* Interleukin-18 overproduction exacerbates the development of colitis with markedly infiltrated macrophages in interleukin-18 transgenic mice. *J. Gastroenterol. Hepatol.* 18, 960–969 (2003).
29. Izcue, A., Coombes, J. L. & Powrie, F. Regulatory T cells suppress systemic and mucosal immune activation to control intestinal inflammation. *Immunol. Rev.* 212, 256–271 (2006).
30. Nakagawa, I. *et al.* Autophagy defends cells against invading group A Streptococcus. *Science* 306, 1037–1040 (2004).

Supplementary Information is linked to the online version of the paper at www.nature.com/nature.

Acknowledgements We are grateful to T. Kitamura, S. Yamaoka and N. Mizushima for providing materials. We thank K. J. Ishii, M. Yamamoto and members of the Laboratory of Host Defense for discussions; Y. Fujiwara, M. Shiokawa, R. Nakayama and N. Kitagaki for technical assistance; and M. Hashimoto and E. Kamada for secretarial assistance. This work was in part supported by grants from NIH (AI070167) and the Ministry of Health, Labour and Welfare of Japan, and by Grant-in-Aid for Specially Promoted Research from the Ministry of Education, Culture, Sports, Science and Technology of Japan.

Author Contributions T.S. generated the Atg16L1-deficient mice and performed the immunological experiments. N.F. performed the cell biology experiments. N.Y. generated the retroviral vector. M.K. and K.T. generated the Atg7-deficient mice. T.T. performed histological analysis of mice. M.H.J., S.U., B.-G.Y., T.S., H.O., T.N., T.K. and O.T. helped with experiments. T.Y. designed the cell biology research. S.A. supervised the overall research project.

Author Information Reprints and permissions information is available at www.nature.com/reprints. Correspondence and requests for materials should be addressed to S.A. (akira@biken.osaka-u.ac.jp).